Dynamics in Drops as Confined Systems Containing Nanoparticles: Reformation of Nanoparticles and Evaporation of Water

Vijitha Mohan, University of Calgary, Calgary, Canada; **Xianjie Qiu**, and **Parthasakha Neogi***, Missouri University of Science and Technology, Rolla, USA

Abstract

Brine is used to displace crude oil in a reservoir and its performance improves when brine contains nanoparticles. It is the presence of nanoparticles in confinements, such as at dynamic contact lines and in thin films, which is of importance. The investigators here have determined a fast way to obtain confined systems by evaporating a small drop of water containing nanoparticles. Water droplets containing nanoparticles of alumina or silica were evaporated on surfaces of polyethylene terephthalate sheets, which are partially wet by water, and glass which is fully wet. After the liquid in the drops evaporated, the residues were examined under a microscope and sintering and melting effects, crystals growth and dendritic formations for alumina and monoliths for silica were seen. The coffee stains are seen in most cases; however measurements show that the contact lines are not always pinned. Turbidity measurements showed that no significant reformation could have taken place in the bulk liquid. A simple model for evaporation, based on geometric measurements, showed that much of the film seen on the solid arose out of evaporation of water that forced the particles down. Sintering rates into the interior could be quantified and shown to be unstable.

Introduction

Deegan and coworkers (Deegan et al. 1997; Deegan et al. 2000; and Deegan 2000) studied small drops of water containing small particles, evaporating from a glass surface. They found that the basal radius of the drop did not change. The particles migrated to the contact line due to a flow that was generated and pinned the foot of the drop there. The rate of evaporation at the contact line was shown to be infinite in a simple model and gave rise to this flow. Much more theoretical and experimental work followed and have been cited in a recent review (Mampallil and Eral 2018). Most work continues to deal with low particle concentrations and/or larger particles. The particles used by Deegan et al. (1997; 2000; Deegan 2000) also showed that the pinning broke down at a very late stage. Their particles were 1μm and, in one case 0.1 μm in diameter, that is, had no Brownian motion (less than 0.1 μm diameters are suggested for significant Brownian motion). The concentrations of the particles were at 2% or less by volume. Researchers have been interested in looking at the effect of nanoparticles (diameters less than 30 nm) at interfaces and in higher amounts for the of crude oil (Bera and Belhaj 2016; Zhang et al. 2014; Cheringhian and Hendraningrat 2018; Ko and Huh 2019). We have examined below, the footprints of evaporating drops of water containing larger amounts of alumina (Al_2O_3) and silica (SiO_2) nanoparticles with water containing 1 wt% NaCl on surfaces of polyethylene terephthalate (PET) and glass. We confine ourselves to liquid-air systems here and not liquid-liquids system in oil recovery because of the ease in achieving films and analyzing the results.

DOI: 10.14800/IOGR.1183

Received January 3, 2021; revised March 2, 2021; accepted April 3, 2021.

*Corresponding author: neogi@mst.edu

Evaporating drops were considered because the dynamics of confined systems in crude oil displacement, such as in thin films and the dynamic contact lines, play key role in the displacement process (Norman 1991). Nanoparticles at large concentrations show extensive reformation. Sintering (Ristić and Milosević 2006) is common. The first layer of molecules on the solid surface is more mobile and can cause two particles to stick. Further, the Laplace pressure, which is the product of curvature and surface tension is very high for the nanoparticles. This gives rise to melting at room temperature and below (Nanda et al. 2003). Finally, as the chemical potentials are high, nanoparticles dissolve faster in the dispersion medium. As a result, the smaller particles dissolve and disappear while the larger ones grow. This is Ostwald ripening (McNaught and Wilkinson 1997). 1% NaCl has been added to water to mimic oil field water, however, it would also discourage Ostwald ripening by reducing the solubility of the solid. Some of these issues have been long known and have been reviewed (Shrestha et al. 2020). We do not know the difference between the behavior in three dimensions versus in two, which is of significance here. We also do not have time scales for comparison.

We have shown below using turbidimetry, that in three dimensions, reformation does not happen over the time scale of interest. We have measured drop dimensions using a contact angle goniometer and used a model to show that the confinement model is good. Finally, we have shown that the footprints left after drying show extensive reformation for which we have identified the ingredients of a quantitative model in one case.

Model

Material Balance. Small drops on a horizontal solid surface have a profile that is a segment of sphere, indicating that the effects of gravity were insignificant. For such a system, the change in water content in the drops is given by:

$$-\rho_L \frac{dV_L}{dt} = Sk_p p_s (1-\phi) e^{\phi}, \quad \text{.....(1)}$$

where V_L is the volume of water in the drop and ρ_L is the density of water. The exponential term has been added on the right following Flory, to take into some effects of higher concentrations. Also *S* is the drop-air interfacial area, k_p is the averaged mass transfer coefficient and p_s is the saturated vapor pressure of water. The term $(1-\phi)$ is the activity, valid in dilute suspensions, and ϕ is the volume fraction of the particles. The total volume is $V = V_L + V_S$where the volume of the solids, $V_S = V_o\phi_o = V\phi$, is a constant. This relationship can be used to track ϕ in **Eq. 1**. The subscript *o* denotes the initial values. Finally, the rate of evaporation is assumed to be distributed instead of being concentrated near the contact line.

A Sedimentation Model. If we assume instead that the concentration of the particles remains constant and that the particles that occupied the evaporated space have been deposited on the solid surface as in sedimentation (Probstein 1994) , we obtain:

$$-\frac{1}{S}\frac{dV}{dt} = \frac{k_p p_s}{\rho_L} e^{\phi_o}, \quad \text{.....(2)}$$

for the deposition model. In a sedimentation experiment, the top of the liquid is clear and the particles have deposited at the bottom. In between, we have the original particle concentrations. Here, we assume that the clear liquid at the top has evaporated away.

Both models given by Eqs. 1 and 2 have two dependent variables each, to be identified later. As a consequence, an additional constraint will have to be sought, possibly from the experimental data to determine the validity of these equations.

Experiments

Materials. NaCl was added to distilled water. Polyethylene terephthalate sheets were cleaned using methanol and, under a microscope, showed sparse sets of scratches. The glass substrate was in the form of coverslips, which being float glass, has roughness less than 2 nm. The coverslips were cleaned with KOH-isopropyl alcohol and then thoroughly rinsed with distilled water. Water does not wet PET and, thus, pinning in some form or other is expected. However, water wets glass and hence pinning will have to overcome spreading. Silica particles had a nominal diameter of 12 nm and the alumina a diameter less than 50 nm. These were used as supplied by Aldrich.

Turbidimetry. The first experiments were to determine how the particles behaved in bulk suspension using a turbidimeter. Water and the particles were mixed and a vibrating table was used to obtain better dispersion. Turbidimeter was calibrated only once using a standard solution. The turbidity of the mixture was measured in the sample holder as a function of time. The results are shown in **Figures 1** and **2**. All particles and many aggregates will be in the Rayleigh scattering regime. Thus, the turbidity (in National Turbidity Units, NTU) will be proportional to the number of scattering centers. However, at the large concentrations used here of 5-50 wt%, multiple scattering will take place, so that the functionality will not be a simple proportionality. At large degrees of aggregation, which occurs because of high concentrations, sedimentation will begin. In general, we see a fine sediment often in 2 hours.

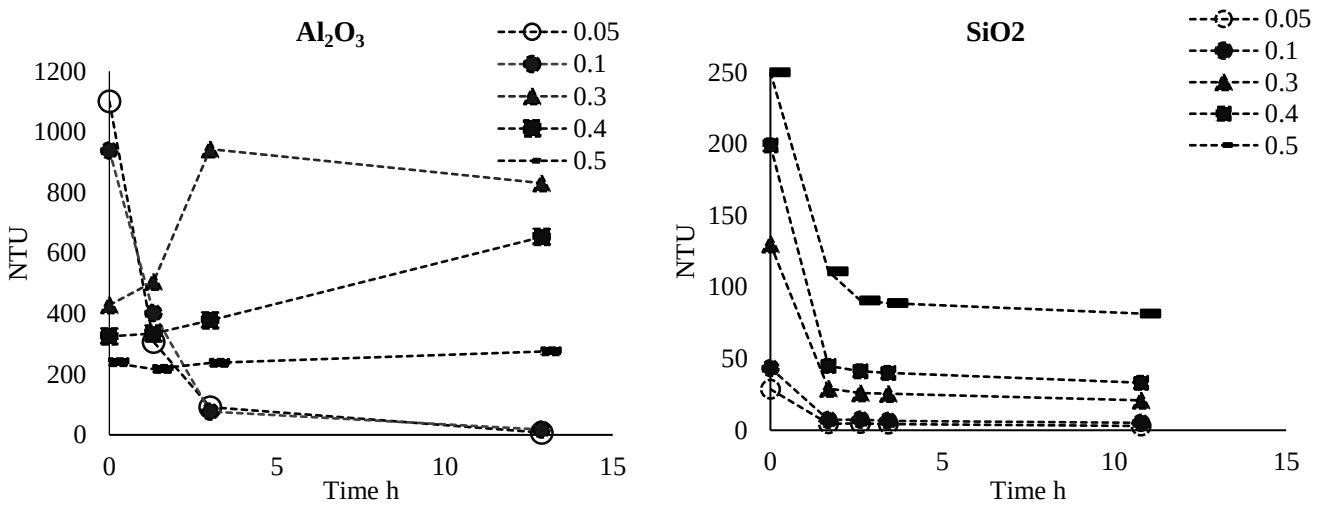

Figure 1—National Turbidity Units NTU as a function of time for alumina and silica at different starting mass fractions. Both figures are plotted with same symbols for the same weight fractions.

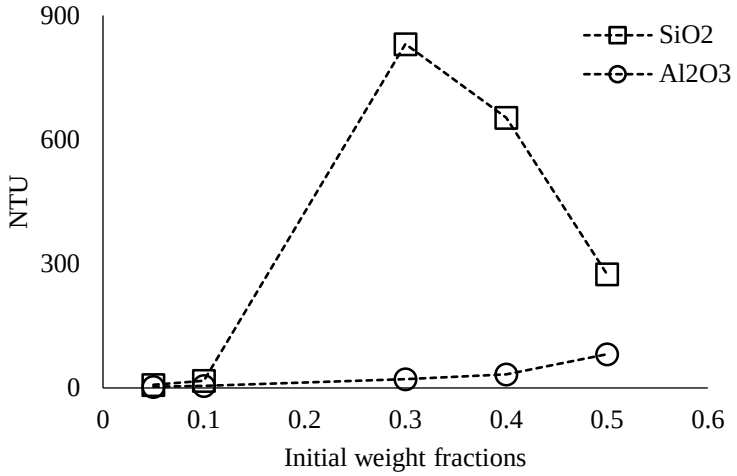

Figure 2—Residual turbidity in National Turbidity Unit NTU of Al_2O_3 and SiO_2. Concentrations are in weight fractions.

Contact Angle Goniometry. The drops of suspensions were layered on the horizontal surface of PET or glass inside the environmental chamber of the Ramé-Hart contact angle goniometer. We needed drops smaller than 10 µl as they are free of the effects of gravity. The drops could not be delivered with the standard microliter syringe and a hypodermic syringe was used. For sufficiently small drops, unaffected by gravity, the drop profiles would have the shape of spherical caps. This was determined by measuring the contact angle α and checking that $\tan(\alpha/2)$=height of the drop at the middle/radius of the base. The two sides of this equation could be obtained independent of one another and compared well. Only a few drops were examined for this sphericity, and data were taken for r_o, basal radius, and α, contact angle, as functions of time. The chamber protects the drop. The best results for the evaporation rates were obtained by keeping the top of the chamber partially open. It was assumed that because of the smallness of the drop, the humidity in the chamber was not too high to affect evaporation. Full evaporation occurred in about 30 minutes. The height of the drop in the middle was monitored to check if full evaporation had taken place. The coverslip was then put in a covered dish and examined under the microscope. During the experiments, the radius of the base was measured to check if pinning occurred.

Results And Discussion

Turbidity. As shown in Figure 1, the turbidity of alumina fluctuates greatly but the turbidity of silica does not and shows a continual decrease with time. Figure 2 shows that two mechanisms may be operating for Al_2O_3. There is another time scale of half an hour, over which the drop evaporates, where a constant value of turbidity can be assumed. It means that the particle microstructures seen in **Figures 3** and **4** are formed after the deposition and not before.

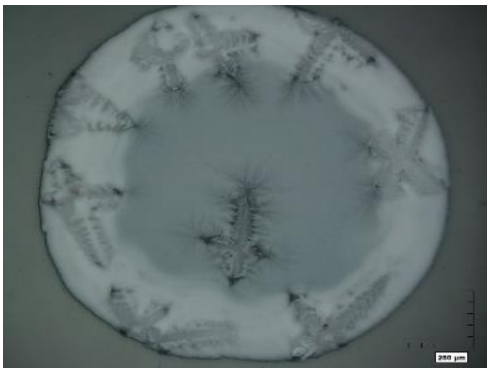

Figure 3—Alumina drop on PET. The bar shown is 250 µm. Initial concentration of alumina is 0.40 weight fraction.

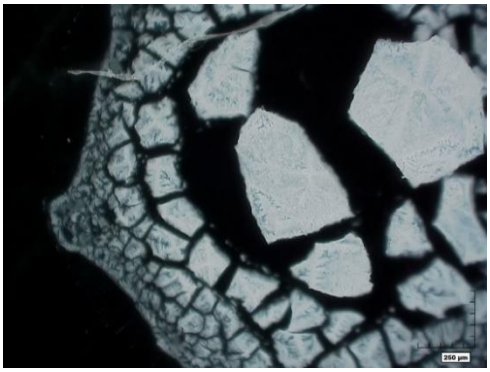

Figure 4—SiO_2 drop on PET. The bar shown is 250 µm. Initial concentration of silica is 0.40 weight fraction.

Analysis of the Evaporation Process. In the next step, the data are analyzed using a sequence that helps us to determine a mechanism. These are in the form of r_o and α as a function of time. Because of the very large amount of data and calculations that result, we have provided the numerical details mainly for two systems below; SiO_2 on glass and Al_2O_3 on PET. Their values of r_o and α are shown in **Figure 5** as functions of time. Shown in **Figure 6** are the volumes calculated from

$$V = \frac{\pi r_o^3}{24}\frac{(2-3cos\alpha+cos^3\alpha)}{sin^3\alpha} \quad \text{.....(3)}$$

We also note that

$$S = \frac{2\pi r_o^2}{1+cos\alpha} \quad \text{.....(4)}$$

Also shown in Figure 6 are the dotted lines that fit to $V = V_o e^{-\omega t}$ which appear to be good. We have added in Appendix why this is expected. This is the additional constraint that we need. We use this fit in Eqs. 1 and 2 to get, for confinement

$$Y = \frac{V/V_o}{\frac{V}{V_o}-\phi_o}\frac{V/V_o}{S/V_o}\omega e^{\phi_o V_o/V} = \frac{k_p p_s}{\rho_L} \quad \text{,.....(5)}$$

and for sedimentation

$$Z = \frac{V\omega}{S}e^{\phi_o} = \frac{k_p p_s}{\rho_L} \quad \text{.....(6)}$$

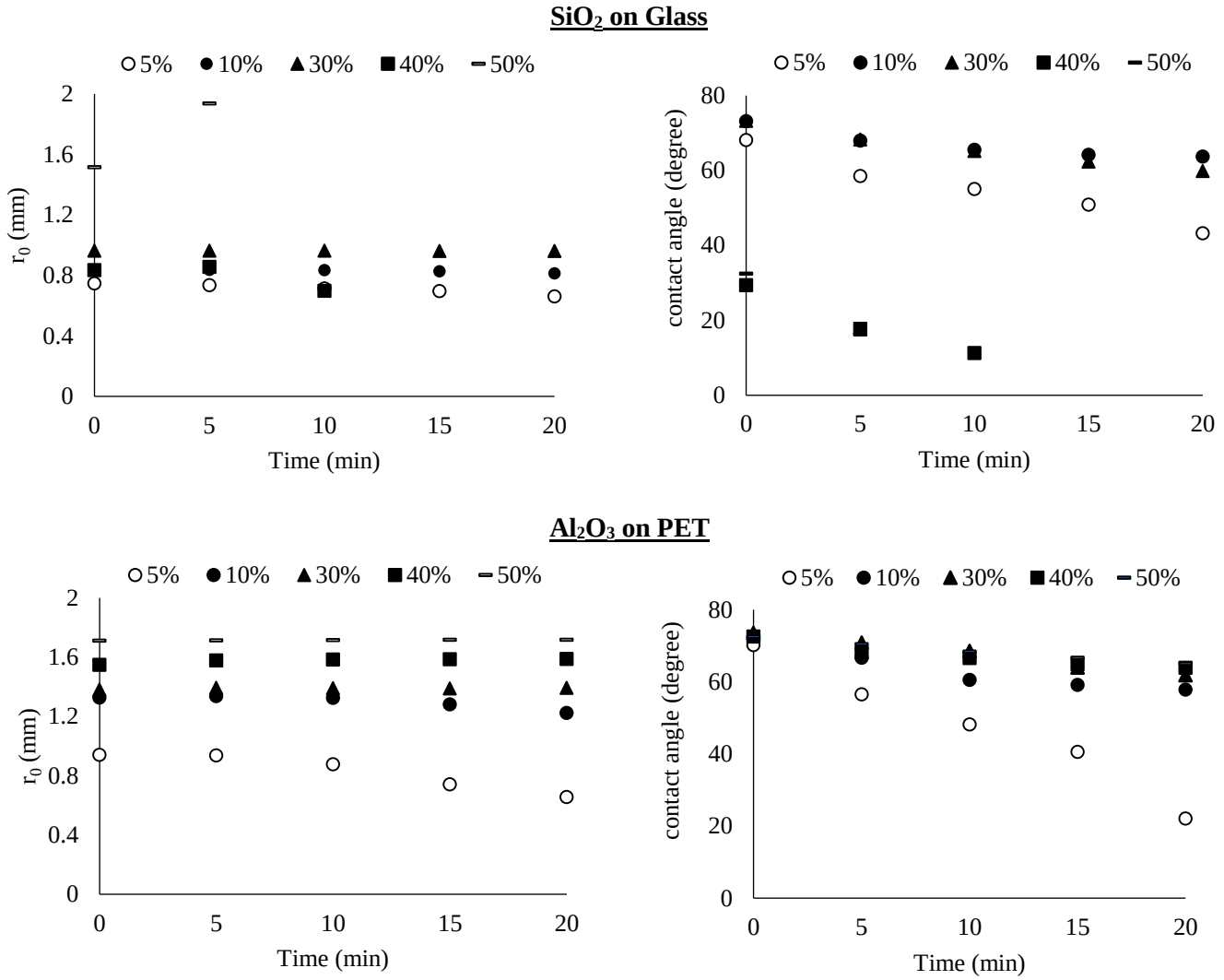

Figure 5—Basal radius r_0 and contact angle α shown for two systems as functions of time. The measurements were taken using a contact angle goniometer. Note that at the smallest concentrations there is a continuous drop in r_0. The measurements were problematic in case of 50 wt% particles.

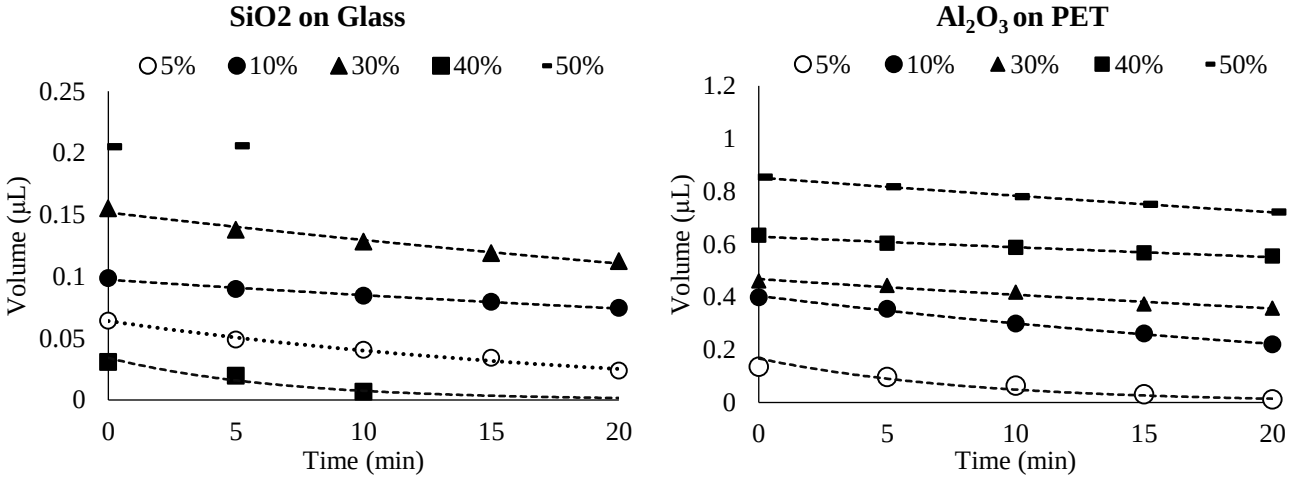

Figure 6—Volumes calculated by assuming that the profiles are given by segments of spheres, and plotted as functions of time. The curves represent exponential fits.

Y as a function of time is plotted in **Figure 7**. Figure 7 shows that all values of *Y* are positive and there are most often independent of time, both expected. For a particular type of nanoparticle, alumina or silica, and for a particular substrate, PET or glass, the plots should be independent of concentrations and coincide. The results are less satisfactory though not too far away. In general, the cases of the top two concentrations show irregularities. When *Z* from Eq. 6 is plotted as a function of time, the plots are spaced even more and show more time dependence. Thus, they have not been shown here, although some effects of sedimentation exist.

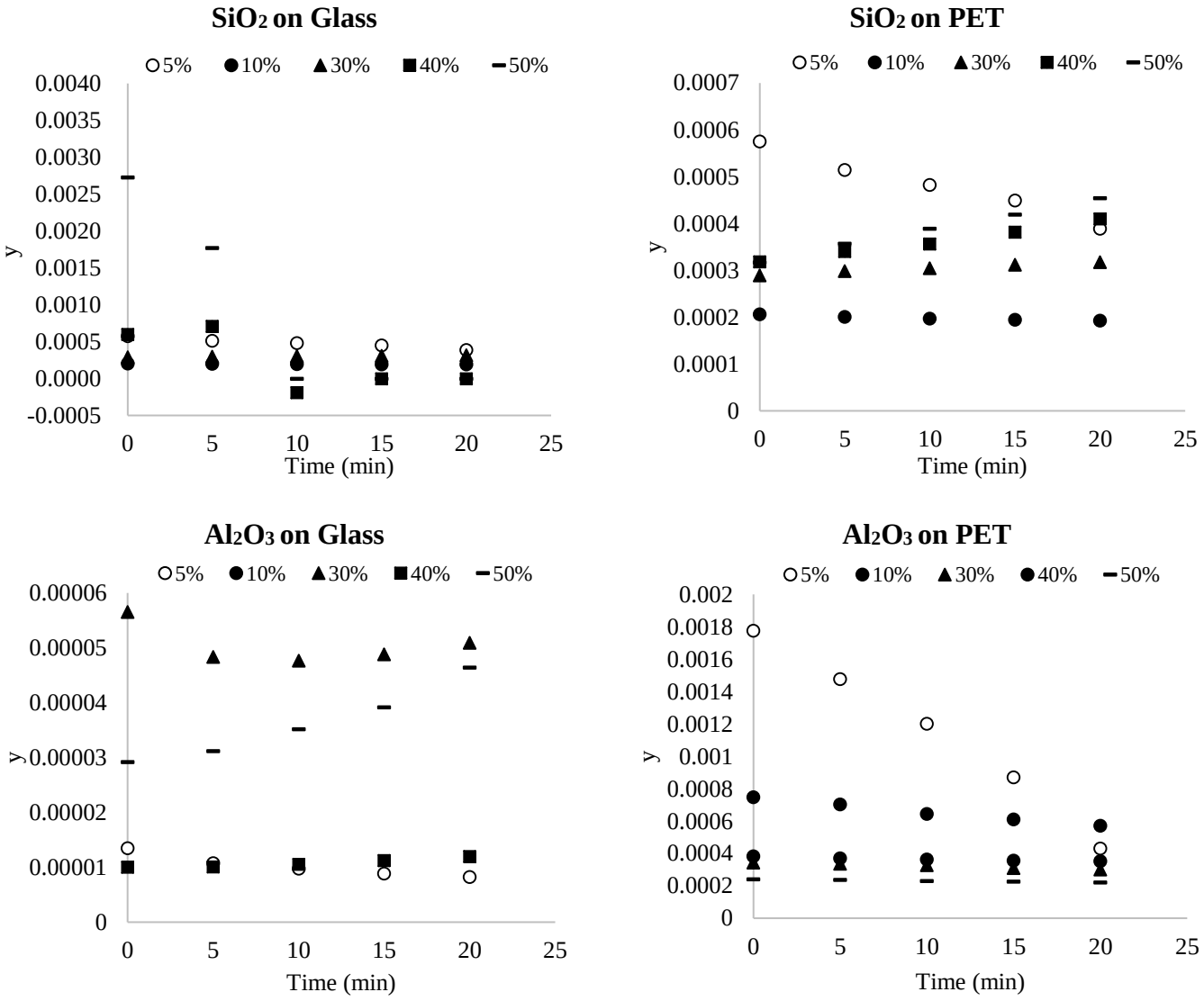

Figure 7—Y in Eq. 5 has been plotted against time for SiO_2 and Al_2O_3 on glass and PET.

On PET, the drops do not spread, that is, the drop border is pinned except for the 5 wt% for silica and 5 and 10 wt% for alumina which retract very slowly at first, then in a significant way at later times (Figure 5). The images of alumina and silica are shown enlarged in Figures 3 and 4 where silica is seen to spread more. The drop edge is practically never smooth but our measurements in Figure 5 do not show fluctuations except at high particle concentrations. Alumina and silica on glass are shown in **Figures 8** and **9**. Both have spread over larger distances such that lower magnification was required to capture the full image.

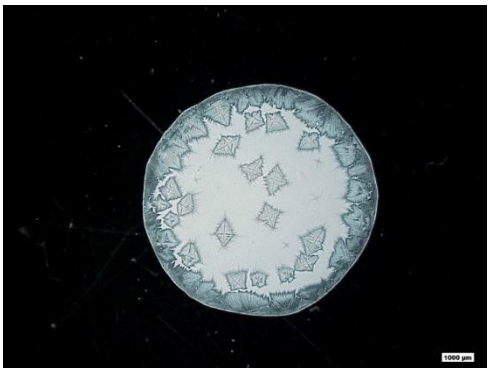

Figure 8—Alumina drop on glass. The bar shown is 1000 μm. Initial concentration of alumina is 0.40 weight fraction.

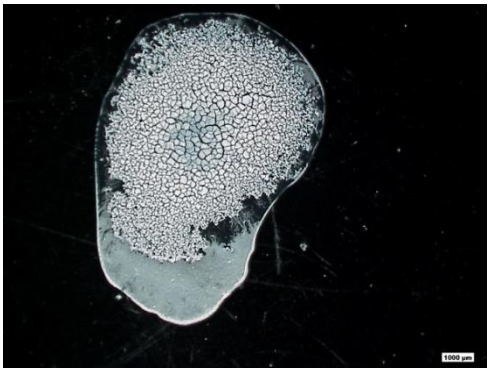

Figure 9—SiO_2 drop on glass. The bar shown is 1000 μm. Initial concentration of silica is 0.40 weight fraction.

Analysis of the Reformation Process. For alumina/PET (Figure 3) and alumina/glass (Figure 8), one can see a moving boundary with the boundary (interline) separating a reformed region from the initial one. The reformed region looks like sintering has happened, that is, nearly uniform and matte. The dynamics of the interline can be expressed through a conservation equation

$$\frac{\partial c}{\partial t} = \frac{D_s}{r}\frac{\partial}{\partial r}\left(r\frac{\partial c}{\partial r}\right), \quad (7)$$

where radial symmetry is being assumed. The concentration c is number of particles per unit area and D_s is the surface diffusivity. It is subject to finiteness and $c = c^*$ a fixed concentration at the interline at $r = r^*$, where particles are converted to a sintered mass (as in alumina/PET Figure 3 or as in alumina/glass Figure 8. A change of variable leads to

$$d\tau = \frac{D_s dt}{r^{*2}}, \quad (8)$$

where $\tau \to 0$ as $t \to 0$ and $\xi = r/r^*$. Taking Laplace transform and inverting using standard tables, one has:

$$\frac{c_\infty - c}{c_\infty - c^*} = 1 - 2\sum_{k=1}^{\infty} \frac{e^{-\lambda_k^2 \tau} J_o(\lambda_k \xi)}{\lambda_k J_1(\lambda_k \xi)}, \quad (9)$$

where c_∞ is the initial concentration, J_i are the Bessel functions and λ_k are the zeros of J_o. The solution is used in the jump balance at the interline

$$R^* = -c^* \frac{dr^*}{dt} - D_s \frac{\partial c}{\partial r}\Big|_{r^*}, \quad (10)$$

where R^* is the rate of sintering in terms of number of particles per unit time per unit interline length and the first term on the right hand side is the effect of moving boundary and is followed by diffusion. Substituting the solution in there we have

$$R^* = -c^* \frac{dr^*}{dt} + 2D_s \frac{c_\infty - c^*}{r^*} \sum \frac{e^{-\lambda_k^2 \tau}}{\lambda_k}, \quad \text{.....(11)}$$

is obtained which gives us an integro-differential equation for r^* as a function of time. An approximation at short times is possible by setting r^* to r_o, the initial drop radius, to calculate $\tau = D_s t / r_o^2$, substituting this τ into **Eq. 11** and then integrating to get a better expression for r^*. However, the diffusion limited growth in a moving boundary problem is often unstable (Probstein 1994). Linear stability analysis that is performed by assuming that the rate of change of interline is much slower than the rate of growth of the instabilities, gives us a fastest growing wavelength, which is the length scale observed in the unstable growth. A length scale can be obtained from the balance between the two rates of mass transfer mechanisms to obtain:

$$\lambda = \frac{D_S (c_\infty - c^*)}{R^*}, \quad \text{.....(12)}$$

which usually differs from the fastest growing wavelength by a dimensionless number of the order of 1. From Figure 3, λ~266 μm, where interline is sinuous suggesting that the instability has just begun. In Figure 8, is 402 μm, where the interline is jagged which cracks separating growth, suggesting that we have looked at the specimen in the late stage of instability. It is noteworthy that in all photographs shown here on silica, the sintering is over and the material has cracked.

On PET, a clear "coffee stain" is seen for alumina, but not as clearly seen in silica as the rim is a lot thinner. Coffee stain refers to the unusually high rates of deposition along the drop periphery. Dendritic growths are common in alumina but not seen as often in silica. In general, dendrites here are due to mass transfer effects that arise from surface diffusivity (Miller 1978) and also known in two dimensions (Neogi and Wang 2011). In addition, large crystals are seen for alumina but not for silica. Silica system shows only small clusters that are barely visible under a microscope. Large crystals are usually due to Ostwald ripening which for, some reason, is more pronounced in alumina. Possibly alumina is more soluble in water.

The very large Laplace pressures, due to the smallness of the particles, can lower the melting point at the surface as stated earlier. In the photographs, the dendrites glisten, which led us to conclude that these are melts.

Finally, we look at the footprints left by the dried drops in all cases for comparison; on PET in **Figure 10** and on glass on **Figure 11**. Systematic changes are seen in all cases with increasing initial concentrations; however, for alumina there is a break between 10 and 30% initial concentrations and such a break also occurs in the turbidimetry results in **Figure 2**.

Nanoparticles show such a high reformation that it is possible to speculate that, in oil reservoirs, they may choke fine pores. In general, the properties of thin films and contact angles will change with time. It also appears that there are significant differences between the footprints left by alumina and by silica, which can be used as markers. However, the main difficulty here is that the process is very fast and may have deleterious effects such as the haphazard nature of reformation. One way of slowing down the system is to add a low molecular weight water soluble oligomer.

Conclusions

All the changes in morphology that were observed could have occurred only on the surface, as demonstrated by the turbidity studies and studies on evaporation rates. Reformation is brought about by sintering and melting, and sintering starts at the coffee stain along the drop periphery and moves inwards. This is the main conclusion, other effects are seen but appear to be secondary.

Dried droplets of Al_2O_3 on PET

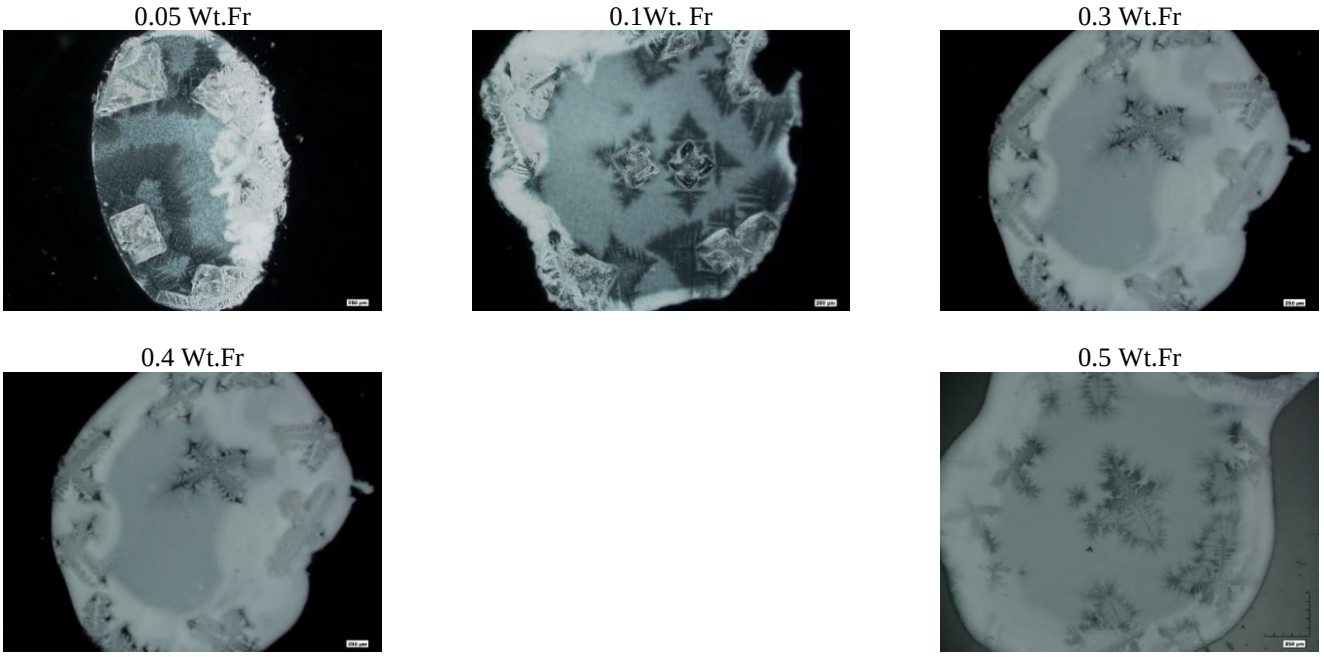

Dried droplets of SiO_2 on PET

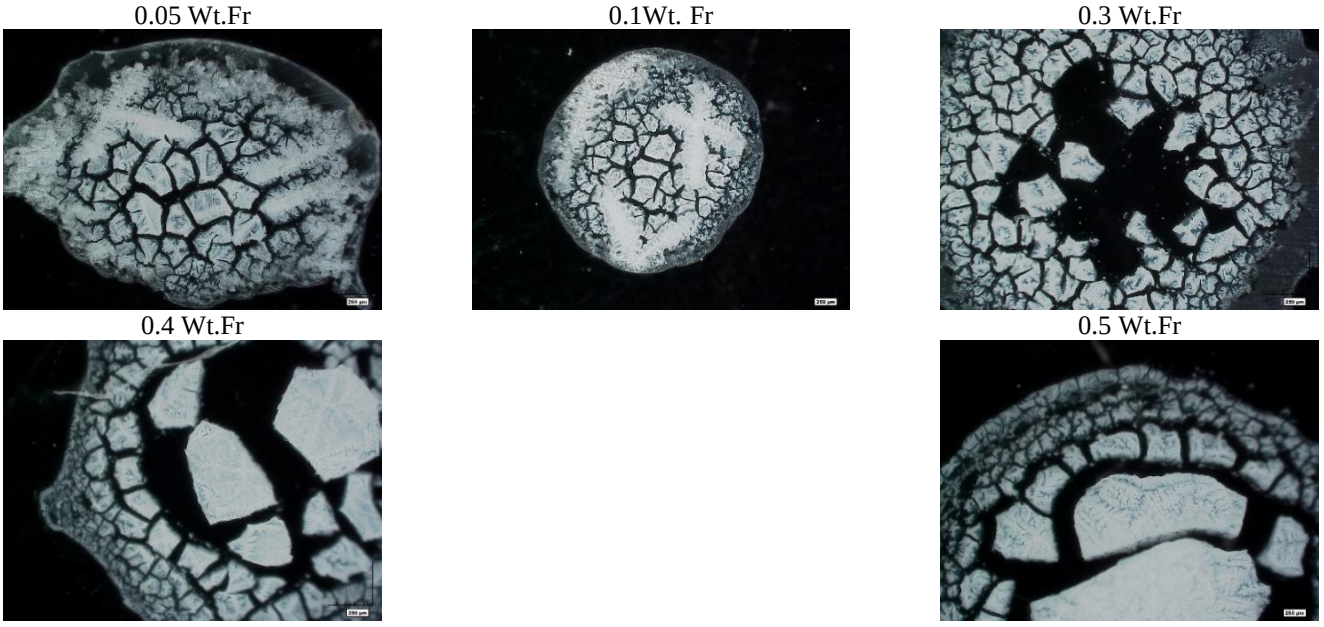

Figure 10—Dried droplets of Al_2O_3 and SiO_2 suspensions where dendrites can be seen in all frames with Al_2O_3 but only in the first two in SiO_2. At lowest concentration of Al_2O_3 we see large crystals. We see coffee stain behavior for Al_2O_3 but it is not so clear in SiO_2. Significant cracks are seen in SiO_2 but not in Al_2O_3. Small white horizontal bars in every frame is 250 µm.

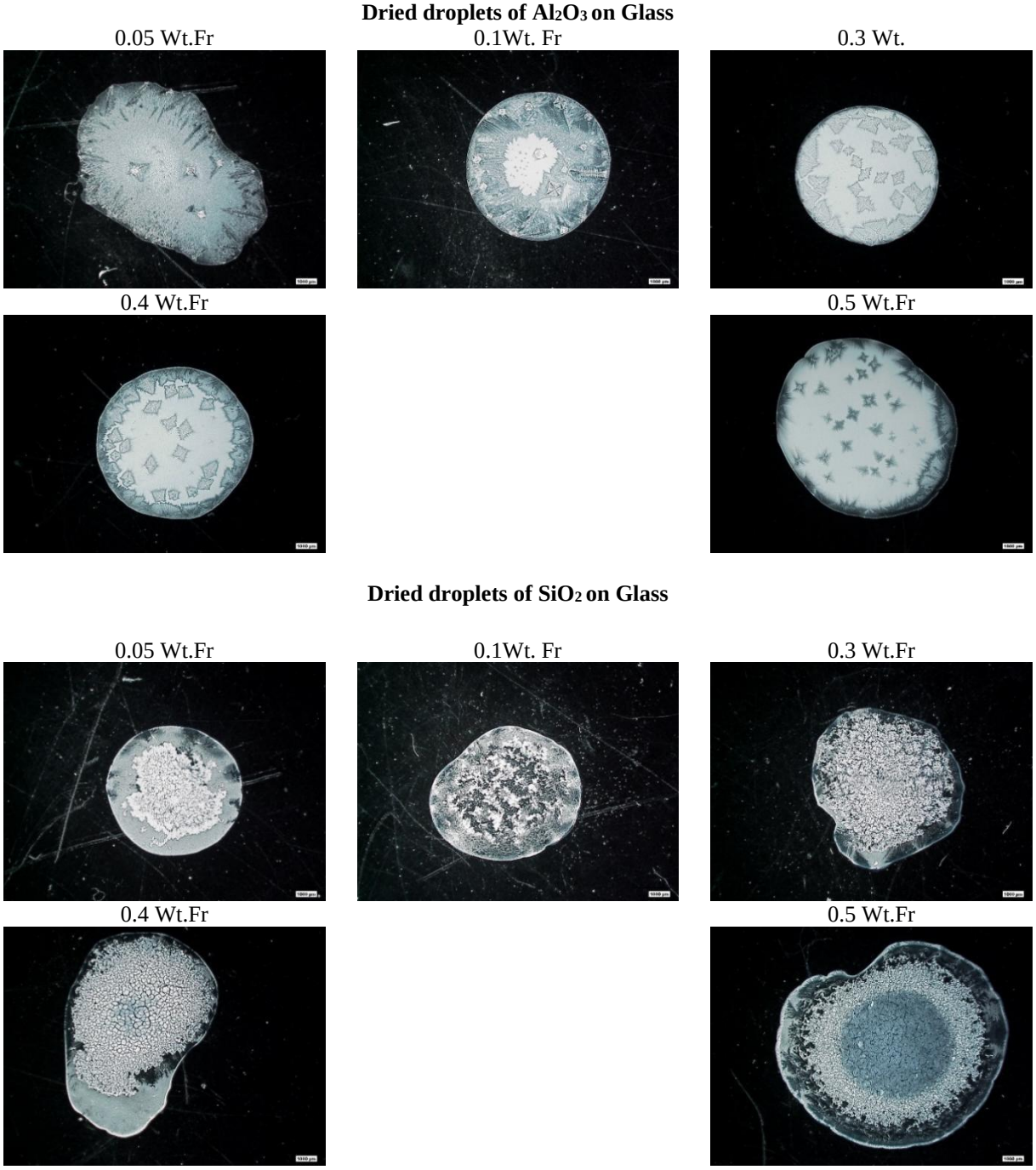

Figure 11—Dried droplets of Al_2O_3 and SiO_2 suspensions where dendrites can be seen only for Al_2O_3 at lower concentration and some at the highest concentration. None appear in SiO_2. Crystals appear everywhere for Al_2O_3 and this feature in not clear in silica. We see coffee stain behavior in all. Small horizontal bar in every frame is 1000 μm indicating larger areas involved due to drop spreading.

Conflicts of Interest

The author(s) declare that they have no conflicting interests.

References

Bera, A. and Belhaj, H.J. 2016. Application of Nanotechnology by Means of Nanoparticles and Nonodispersions in Oil Recovery. *Nat. Gas Sci. Eng*. **34**: 1284-1309.

Cheringhian, G. and Hendraningrat, L. 2018. A Review on Applications of Nanotechnology in Enhanced Oil Recovery Part B: Effects of Nanoparticles on Flooding. *Int. Nano Letts*. **6**: 1-10.
Deegan, R.D. 2000. Pattern Formation in Drying Drops. *Phys. Rev. E*. **61**: 475-48.
Deegan, R.D., Bakajin, O., Dupont, T.F., et al. 1997. Capillary Flow as the Cause of Ring Stains from Dried Drops. *Nature* **389**: 827- 829.
Deegan, R.D., Bakajin, O., Dupont, T.F., et al. 2000. Contact Line Deposits in an Evaporating Drop. *Phys. Rev. E.* **62**: 756-765.
Ko, S. and Huh, C. 2019. Use of Nanoparticles in Oil Recovery. *J. Pet. Sci. Tech*. **172**: 97-114.
Mampallil, D. and Eral, H.B. 2018. A Review on Suppression and Utilization of the Coffee-Ring Effect. *Advances in Colloid Interface Science* **252**: 38-54.
McNaught, A.D. and Wilkinson, A. 1997.*Compendium of Chemical Technology*. 2nd ed. Oxford: Blackwell Scientific Publications.
Miller, C.A. 1978. *Stability of Interfaces, in Surface and Colloid Science*, Matijevic, E., ed. New York: Plenum Press.
Nanda, K.K., Sahu, S.N., and Behera, S.N. 2002. Liquid Drop Model for the Size-Dependent Melting of Low-Dimensional Systems. *Phys. Rev. A*. **66**: 193-208.
Neogi, P. and Wang J.C. 2011. Stability of Two-Dimensional Growth of A Packed Body of Proteins on A Solid Surface. *Langmuir* **7**: 5347-5353.
Norman, R.M. and Dekker, M. 1991. *Interfacial Phenomena in Petroleum Recovery*. New York: Marcel Dekker.
Probstein, R.F. 1994. *Physicochemical Hydrodynamics*. 2nd ed. New York: John Wiley and Sons.
Ristić, M.M. and Milosević, S.D. 2006. Frenkel's Theory of Sintering. *Science of Sintering* **38**: 7-11.
Shah, R. and Neogi, P. 2002. Interfacial Resistance in Solubilization Kinetics. *J. Colloid Interface Sci* **253**: 443-454.
Shrestha, S., Wang, B., and Dutta, P. 2020. Nanoparticle Processing: Understanding and Controlling Aggregation. *Adv. Colloid Interface Sci*. **279**:102-122.
Zhang, H., Nikolov, A., and Wasan, D. 2014. Enhanced Oil Recovery (EOR) Using Nanoparticle Dispersions: Underlying Mechanism and Imbibition Experiments. *Energy Fuels* **28**: 3002-3009.

Appendix

Previously for a drop of oil on a solid disappearing under surfactant solution, (Shah and Neogi 2002) we had assumed for the conservation equation Eq. 1 that $S \propto V^{2/3}$ and obtained excellent results. This is not a first order processes. Shah and Neogi (2002) calculated the proportionality constant numerically but found that it failed for flat and thin drops. For this case where drops are flat and thin, Eqs. 3b and 4b can be combined to show that $V = \frac{h}{2}S$or $V = \frac{<h>}{2}S$ where $< h >$ is an appropriate average height at the center of the drop. Here, we have

$$V = \frac{\pi}{3}h^2(3R - h), \quad \text{(A-1)}$$

$$S = 2\pi Rh \quad \text{(A-2)}$$

We calculated *V*/*S* and found the ranges in the four cases to be narrow. They range from 0.0258 to 0.0341, 0.0258 to 0.0356, 0.0100 to 0.0224 and 0.0357 to 0.0545 mm, for SiO_2 (on glass then on PET) followed by Al_2O_3 in the same order. 5% solids was always an outlier, showing twice as much change. The systems at 40% and 50% were erratic and were not considered. It is seen that *V*/*S* can be approximated as a constant which when substituted in Eq. 1 leads to $V = V_o e^{-\omega t}$used after Eq. 4.

Vijitha Mohan received her Ph.D. in Chemical Engineering from Missouri University of Science and Technology and served as a Lecturer after graduation. Her research interests lie in heavy oil recovery. She acquired her B.Tech in Chemical Engineering from University of Madras and M.S in Chemical Engineering from Mississippi State University. She is at present a Postdoctoral Associate at University of Calgary, Canada.

Xianjie Qiu received the Ph.D., master and bachelor's degree in Chemical Engineering Department from Missouri University of Science and Technology. His research interests in convective-diffusive transport.

Parthasakha Neogi, is a Professor of Chemical Engineering at Missouri University of Science and Technology, where he has worked as faculty for the last 36 years. His research interests are in wetting, surfactants and polymers, and in interfacial transport phenomena. He holds B.Tech. (Hons.) from the Indian Institute of Technology Kharagpur, M. Tech. from the Indian Institute of Technology Kanpur, and Ph.D. from Carnegie-Mellon University, all in chemical engineering.